DOI: 10.24874/ti.2171.04.26.06

Tribology in Industry

www.tribology.rs

RESEARCH

Investigation of Failures in a Belt Conveyor Shaft Coupled by an Expansion Ring

Caio Machado Bertholdi[a], Gustavo Tressia[b,*]

[a]*Vale S.A, Vitória, ES, Brazil,*
[b]*Instituto Tecnológico Vale, Ouro Preto, MG, Brazil.*

Keywords:

Fretting wear
Fretting fatigue
Conveyor belt
Shaft failure
Expansion ring

* Corresponding author:

Gustavo Tressia
E-mail: gustavo.tressia@itv.org

Received: 3 April 2026
Revised: 26 May 2026
Accepted: 23 June 2026

ABSTRACT

This study presents a failure analysis of a conveyor pulley shaft belt that experienced recurrent fatigue fractures at the contact region with an expansion ring. The investigation combined non-destructive testing, fractographic analysis, scanning electron microscopy, mechanical characterization, and fracture mechanics–based evaluations to identify the failure mechanism and root cause. Chemical and mechanical analyses confirmed that the shaft material complies with SAE 4340 steel specifications and exhibits adequate static strength, fracture toughness, and fatigue resistance under nominal design conditions. Surface analyses revealed clear evidence of fretting wear, including adhesive junctions, abrasion marks, and plastic deformation, indicating a tribological damage mechanism dominated by micro-slip under high contact pressure. Fracture mechanics assessments showed that surface defects on the order of 0.113 mm are sufficient to propagate under the applied cyclic stresses. Crack growth analysis based on the Paris law indicated that once initiated, a fatigue crack could reach a critical size in seven days of operation. The results demonstrate that the failure was caused by fretting fatigue promoted by localized contact stresses and relative micro-sliding at the interference-fitted interface. The findings highlight the importance of controlling fretting damage and provide a quantitative basis for defining design improvements and maintenance strategies for conveyor pulley shaft systems.

1. INTRODUCTION

Belt conveyors are widely used for the transportation of bulk materials and play a critical role in industries such as mining, agriculture, and food processing. These systems have been increasingly adopted for long-distance material handling due to their ability to significantly reduce operational costs and environmental impacts when compared to conventional transportation methods, such as truck haulage. In specific applications, conveyor belt systems can reach total lengths of up to 100 km, highlighting their strategic importance in large-scale logistics and material handling operations [1,2].

In many industrial applications, belt conveyor systems operate as a single, continuous material handling line, often representing the sole means of material flow within the production process. Under such conditions, failures in individual components, maintenance interventions—particularly unplanned ones—and operational shutdowns lead to the immediate interruption of the entire conveying system. This scenario directly affects production and may result in substantial financial losses, especially in large-scale, high-capacity operations. Within this context, the need for systematic failure analysis studies becomes evident, aiming to identify degradation mechanisms, root causes, and recurring failure modes, thereby contributing to improved operational reliability, equipment availability, and overall system safety.

One of the main components of a belt conveyor system is the conveyor pulley, which is responsible for transmitting torque to the belt or for redirecting the belt along the conveyor path. Drive pulleys (head pulleys) are designed to transmit power from the drive system to the belt through frictional contact, while non-driven pulleys, such as tail, snub, and take-up pulleys, are primarily used to change the belt direction, increase wrap angle, and maintain adequate belt tension [3].

From a structural standpoint, a conveyor pulley is typically composed of a shell (drum), end disks or diaphragms, hubs, shaft, and bearing assemblies, all of which are subjected to complex combinations of bending, torsional, and cyclic stresses during operation. The shaft-to-hub connection in conveyor pulleys is commonly achieved through locking assemblies or keyed connections, with the selection dependent on the mechanical and operational requirements of the application.Due to the continuous rotation under fluctuating belt tensions, pulleys operate under high-cycle fatigue loading, making them critical components from a reliability and failure analysis perspective [4,5].

Conveyor pulley failure modes reported in the literature include fatigue cracking of the pulley shaft, often initiated at geometric stress concentrators such as diameter transitions or keyways; shell rupture or cracking due to insufficient shell thickness or excessive belt tension; and weld-related failures in end disks or shell-to-diaphragm connections [5-8]. In particular, inadequate design parameters, deviations from recommended CEMA [3] practices, improper reconditioning, or unforeseen operating conditions have been identified as primary contributors to premature pulley failures, frequently resulting in unplanned downtime and significant production losses.

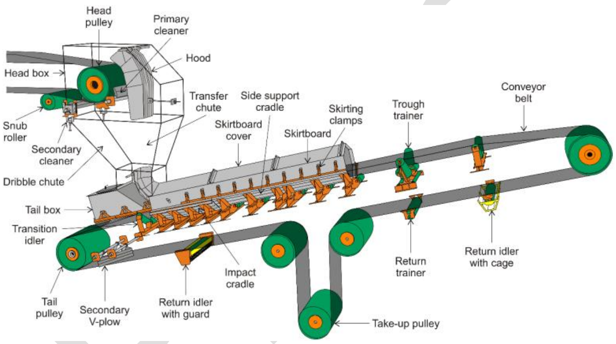

Fig 1. Belt conveyor system [1].

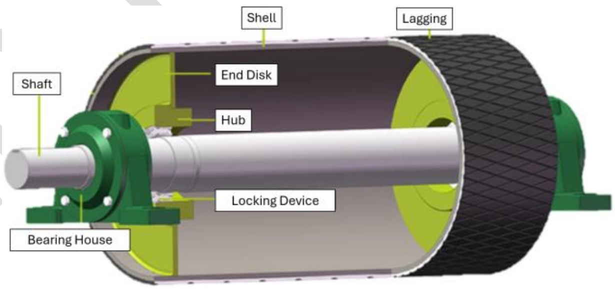

Fig. 2. Conveyor pulley [2].

Figure 1 presents an overall view of a conveyor belt system, while Figure 2 illustrates a typical conveyor pulley assembly and its main components. The aim of this study is to conduct a failure analysis of a belt conveyor pulley shaft by characterizing the fracture mechanisms and features, with the objective of identifying the root cause of the failure. In such systems, tribological phenomena at shaft–hub interfaces, particularly fretting wear and fretting fatigue, represent critical but often underestimated failure mechanisms, especially in interference-fitted assemblies subjected to cyclic loading.

1.1 Contextualization

This work presents a failure analysis motivated by a series of failures that occurred in the shaft of a belt conveyor pulley. All failed shafts were supplied by the same manufacturer and installed under identical operating and assembly conditions. In addition, all shafts were coupled to the drum hubs using the same expansion ring design, which applies an assembly contact pressure of 254 MPa. The nominal contact pressure of 254 MPa corresponds to the assembly specification provided by the expansion ring manufacturer, based on tightening torque and ring geometry. These failures were classified as critical because the conveyor operates as a single conveying line, directly connecting the mining operation to the mineral processing plant. The conveyor belt under investigation has a total length of approximately 10 km, downhill elevation of almost 300 m, 5,4 m/s belt speed and design capacity of 21.000 t/h, such that any unplanned shutdown results in immediate and significant production losses.

A total of four (4) failures occurred in the same location, specifically in the region of the locking assembly (expansion ring) responsible for connecting the shaft to the pulley hub. The mean time to failure (MTTF) of the shafts was approximately 345 days. In order to enable a more accurate identification of the failure origin, a shaft that had not fractured completely was selected for detailed analysis. Although this shaft remained partially intact, a crack was clearly identified in the same region where complete fractures had previously occurred.

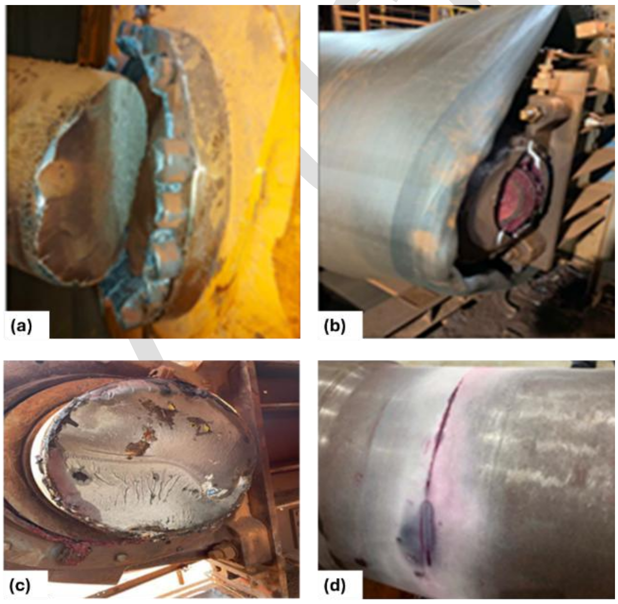

Fig. 3. (a) and (c) Example of fractured shaft of the conveyor pulley, (b) belt misalignment after fractured shaft and (c) selected shaft for failure analysis.

Figure 3a and Figure 3c show conveyor pulley that experienced complete fracture, as a consequence of the fracture, the conveyor belt shifted laterally, resulting in belt misalignment (Figure 3b). Figure 3d presents the shaft selected for analysis, in which the crack can be clearly observed at the contact region between the shaft and the locking assembly.

2. EXPERIMENTAL PROCEDURE

A shaft that exhibited crack formation during service, yet did not undergo complete fracture, was selected for analysis.; a crack was identified in the region corresponding to the contact with the locking assembly (expansion ring), which is the same location where fractures occurred in other conveyor pulleys. This approach was adopted under the assumption that the analysis of a partially damaged component could provide relevant evidence to identify the characteristics associated with the initiation of the failure.

Fig. 4. The selected shaft.

The selected shaft is shown in Figure 4. Initially, the shaft was inspected using liquid penetrant testing in order to detect the presence of cracks (arrow red) and to allow their identification and dimensional characterization. Subsequently, the shaft was sectioned for further examination. Two regions of the shaft were analyzed, both located within the contact zone with the locking assembly. One region corresponded to the area where the crack was detected, while the second region, positioned at the opposite side of the shaft circumference, did not present any visible cracking. Figure 5 illustrates the drawing of the conveyor pulley where the shaft was installed, with emphasis on the area of interest of this study, corresponding to the shaft region in contact with the locking assembly.

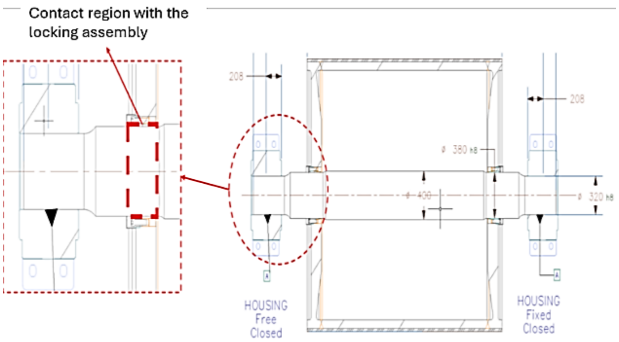

Fig. 5. Schematic representation of the conveyor pulley showing the application of the shaft analyzed in this study.

Leave one clear line before and after a main or After sectioning the shaft into smaller specimens from each region, the samples were initially examined using a stereomicroscope to identify surface features and existing defects. Subsequently, the specimens were analyzed using a scanning electron microscope (SEM) (JEOL IT-200) to identify micromechanisms of wear as well as the associated failure mechanisms.

Microstructural analyses using SEM were performed in the regions corresponding to crack initiation and propagation, aiming to correlate microstructural features with the origin of the crack. For microstructural examination, the samples were initially mounted in bakelite, followed by grinding with #220, #400, #600, and #1200 grit abrasive papers, and polishing with diamond suspension down to 1 µm. The microstructure was revealed using a 2% Nital etchant.

Hardness measurements were carried out using the Vickers method on the transverse section of the shaft, including regions with and without cracks, as well as a region located away from the contact with the locking assembly. Tensile tests were performed according to ASTM E8-21 [9] using an Instron 2382 testing machine. To evaluate the impact resistance, Charpy tests were carried out at a Time JB300 equipment with a 300 J hammer and type A specimens, as stipulated by ASTM E23 [10]. Three repetitions were performed.

The shaft was also subjected to chemical analysis. The carbon and sulfur contents were determined by direct combustion analysis using a LECO CS-300 analyzer. The concentrations of the remaining alloying elements were obtained by optical emission spectrometry (spark OES) using an Anacom Científica B2ADV spectrometer.

3. RESULTS

The steel used in the manufacture of the shaft exhibits chemical composition and mechanical properties consistent with SAE 4340 steel, as shown in Table 1 and Table 2, respectively.

Table 1. Chemical composition of the shaft.

(%)								
C	**Si**	**Mn**	**P**	**S**	**Cr**	**Ni**	**Mo**	**Fe**
0,43	0,25	0,69	0,011	0,008	0,72	1,74	0,25	remain

Table 2. Mechanical properties of the shaft.

Hardness (HV)	**Tensile Test**			**Charpy (J)**
	Ys (MPa)	**UTS (MPa)**	**El (%)**	
261 ± 2	706 ± 11	899.6 ± 9	21.6 ± 2	61 ± 2

After sectioning the conveyor pulley shaft, the region of interest was examined by liquid penetrant testing. A crack extending over approximately one-third of the shaft circumference was identified, as illustrated in Figure 6.

A new cut was performed in order to expose the crack and enable a more detailed visual analysis of the fractured surface (Figure 7). A typical fatigue fracture was observed, with the presence of beach marks (yellow) and ratchet marks (green). Ratchet marks are formed when two cracks nucleated on slightly different planes coalesce, creating a step on the fracture surface. Therefore, a crack nucleation site is expected to exist between two ratchet marks (blue arrows).

Fig. 6. Conveyor pulley shaft examined with liquid penetrant test.

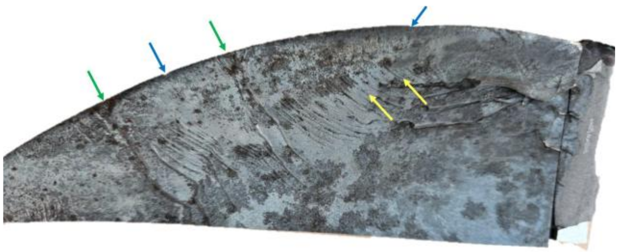

Fig. 7. Conveyor pulley shaft fractured surface.

Near the fracture on the shaft surface, a highly roughened morphology is observed, likely resulting from contact with the expansion ring. This region is characterized by the presence of scratches, microcavities, grooves, and secondary microcracks, which are indicative of a probable fretting mechanism (black arrows). The increase in surface roughness caused by the wear process contributes to the nucleation of fatigue cracks. No evidence of a third-body presence was identified, ruling out possible contamination by ore particles. In addition to the wear process, the expansion ring exhibits an extremely localized contact with the shaft, resulting in an additional stress concentrator that acts synergistically in promoting failure. Figure 8 shows the shaft surface area near the fracture region with a roughened appearance, indicating a possible occurrence of fretting at the contact interface between the shaft and the expansion ring.

A SEM (Scanning Electron Microscopy) surface analysis performed at the crack nucleation region (Figure 9) revealed microcracks (orange arrows), plastic deformation (white arrows), adhesive junctions (purple arrows), and abrasion scratches (black arrows). These features are characteristic of a fretting damage mechanism arising from small-amplitude oscillatory motion under high contact pressure between the shaft and the expansion ring. The repeated micro-sliding at this highly localized interface promotes adhesive and abrasive wear, leading to progressive surface degradation, localized plastic deformation, and the formation of secondary microcracks. Such damage mechanisms increase local stress concentration and act as preferential sites for fatigue crack nucleation.

The occurrence of fretting requires relative microsliding at the contact interface, which may arise even in interference-fitted assemblies due to non-uniform contact pressure, surface roughness, and local elastic-plastic deformation. In addition, cyclic bending and torsional loading during operation can lead to periodic variations in contact stress, promoting micro-slip at the interface. Small deviations in assembly conditions, such as uneven tightening or surface irregularities, may further intensify this effect, contributing to the initiation of fretting damage.

Consistent with the observations near the fracture surface discussed previously, the SEM analysis of the region adjacent to the crack nucleation site revealed the same damage features, namely microcracks (orange arrows), plastic deformation (white arrows), adhesive junctions (purple arrows), and abrasion scratches (black arrows), as shown in Figure 10. The recurrence and spatial continuity of these features indicate that the fretting process was not confined to a single point but rather extended over the contact area imposed by the expansion ring.

The contact between the shaft and the expansion ring is characterized by high contact pressures (≈254 MPa) combined with cyclic loading, creating conditions favorable for fretting wear. Under such conditions, small-amplitude oscillatory motion leads to the formation of adhesive junctions, which repeatedly form and break during service. This process results in surface damage through adhesive and abrasive wear mechanisms.

In addition, the presence of repeated micro-slip may promote the formation of tribolayers and oxidized debris, although no significant third-body accumulation was observed in this study.

The observed combination of plastic deformation, microcracking, and surface roughening is consistent with classical fretting regimes under partial slip conditions, in which localized stick-slip behavior leads to high stress gradients and accelerated fatigue crack initiation.

The extremely localized contact imposed by the expansion ring acts as an additional stress concentrator, which, when combined with fretting-induced surface damage, creates favorable conditions for fretting fatigue. The synergistic interaction between localized contact stresses, wear-induced roughness, and cyclic loading accelerates crack initiation and supports early crack propagation, ultimately leading to fatigue failure of the shaft.

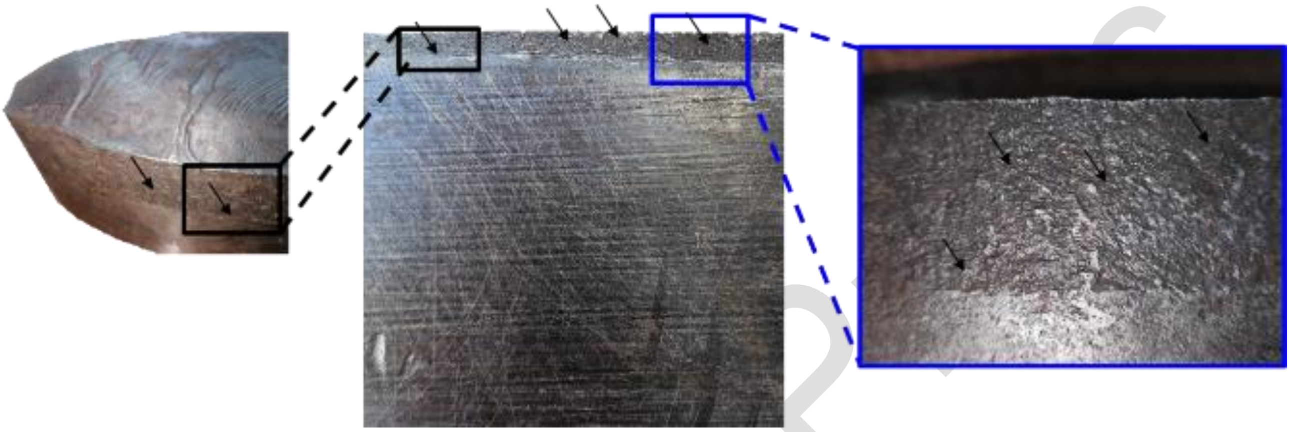

Fig. 8. Rough region on the surface of the shaft.

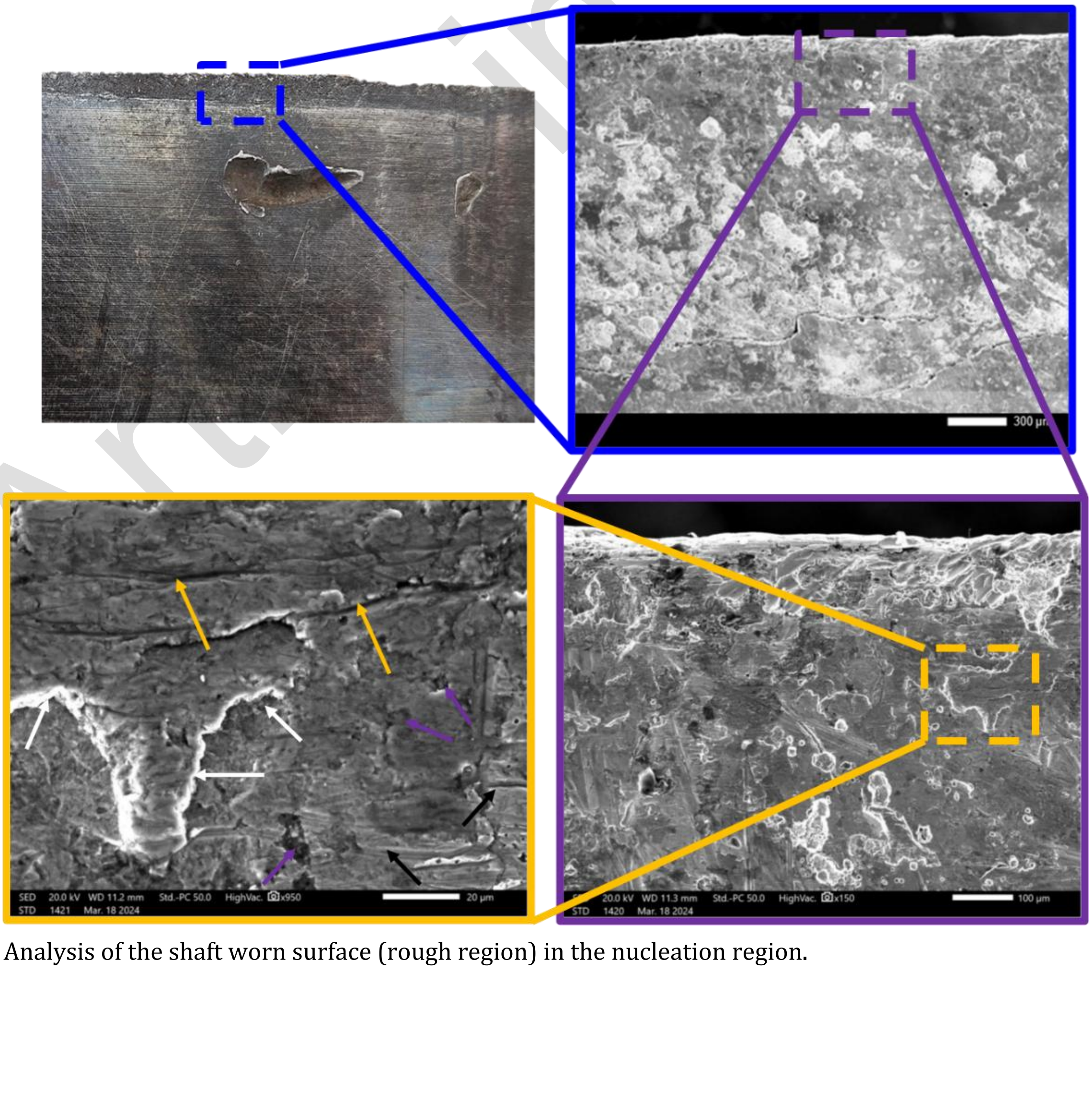

Fig. 9. Analysis of the shaft worn surface (rough region) in the nucleation region.

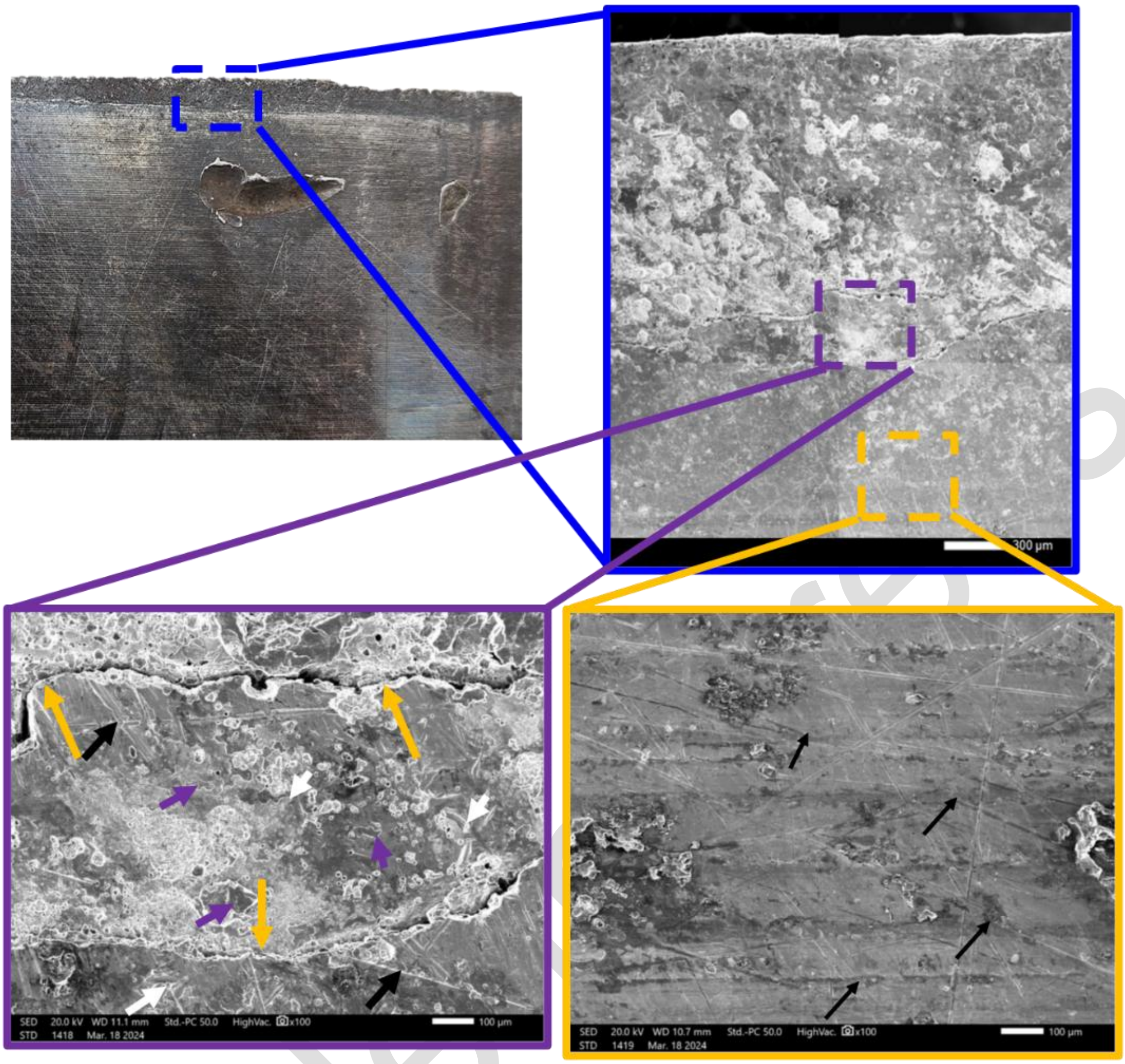

Fig. 10. Analysis of the shaft wear surface (rough region) in the region adjacent to the nucleation region.

To achieve a better understanding of the failure mechanism, a stress analysis was performed in order to assess the adequacy of the original design conditions. As an initial step, the fracture toughness of the shaft material was estimated using the equation proposed by Rolfe and Barson [11], which allows the determination of fracture toughness (K_{Ic}) based on the material yield strength (Ys) and Charpy impact energy (CI), by applying Equation (1) with the material properties listed in Table 2, the calculated fracture toughness of the shaft material was found to be 157 MPa·m^(1/2). The fracture toughness value K_{Ic} is related to the applied remote stress σ through the Irwin relationship (1960), as expressed in Equation (2), where a represents the crack length and Y is the geometric correction factor. This relationship establishes the direct link between the material's resistance to crack propagation and the local stress state acting at the crack tip. According to Skinn et al. [12], for a crack in a solid shaft subjected to bending stresses, the geometric factor can be calculated using the equations presented in Equation 3, where F is the geometric factor, a is the final crack length, and D is the shaft diameter. The crack length measured on the fracture surface was approximately a = 190 mm (0.19 m), and the shaft diameter was 380 mm. Substituting these values into the Equation 4, Equation 5 and Equation 6 results in a geometric factor of Y = 0.86.

With the crack size (a), the material fracture toughness (K_{Ic}), and the geometric factor (Y), it is possible to determine the maximum remote stress applied to the shaft at the moment of fracture. Using the equation presented in Equation 2, the calculated stress (σ) value was 235 MPa.

$$K_{Ic} = Ys \,.\, \sqrt{0{,}646 \,.\, \frac{CI}{Ys} - 0{,}01} \quad (1)$$

$$K = F \,.\, \sigma \,.\, \sqrt{\pi\, a} \quad (2)$$

$$F = G \,.\, (0.923 + 0.199.Y) \quad (3)$$

$$G = 0.92 \left(\frac{2}{\pi}\right) \sec\beta \left(\frac{\tan\beta}{\beta}\right) 1/2 \quad (4)$$

$$Y = 1 - \sin\beta \quad (5)$$

$$\beta = \left(\frac{\pi}{2}\right)\left(\frac{a}{D}\right) \quad (6)$$

The calculated stress corresponds to the remote applied stress, denoted as σ, acting on the shaft. In the crack initiation region, a stress concentration effect is present due to the interference-fitted expansion ring. Based on literature data for interference-fitted components [13], a stress concentration factor (Kt) of approximately 2 was assumed. Thus, the maximum local stress at the crack initiation site can be estimated as:

$$\sigma_{local,max} = K_t \cdot \sigma \quad (7)$$

resulting in σlocal,max ≈ 470 MPa.

According to fracture mechanics–based estimations, considering the crack size (a), the fracture toughness (K_{IC}), and the geometric factor (Y), the maximum local stress acting on the shaft at the crack initiation region was estimated to be σlocal,max ≈ 470 MPa.

The static safety factor (n) is defined as the ratio between the material yield strength (Ys) and the maximum local stress, and is given by:

$$n = \frac{Ys}{\sigma_{local,max}} \quad (8)$$

Considering a yield strength of Ys = 706.6 MPa for the shaft material and a maximum local stress of σlocal,max = 470 MPa at the shaft surface in contact with the expansion ring, the resulting static safety factor is n ≈ 1.5. Therefore, from a static loading standpoint, the shaft material exhibits an acceptable safety margin for operation.

The fatigue limit is defined as the stress level below which no failures occur under laboratory testing conditions. Based on CEMA (2014), the fatigue limit of the drum shaft can be estimated using the following relation (Equation 9):

$$S_f = K_a \cdot K_b \cdot K_c \cdot K_d \cdot K_e \cdot K_f \cdot K_g \cdot S_e' \quad (9)$$

where Sf is the corrected fatigue limit of the shaft and Sf* is the ultimate fatigue limit of the shaft material. The correction factors are defined as follows: Ka is surface finish factor, assumed as 0.8 for a machined shaft; Kb is size factor, given by Kb = $1.85 \cdot D^{-0.19}$, where D is the shaft diameter (in millimeters); Kc is reliability factor, assumed as 0.897; Kd is temperature factor, equal to 1.0 for operating temperatures between −57 °C and 204 °C; Ke is load cycle factor, assumed as 1.0 when the stress does not exceed the ultimate strength; Kf is stress concentration factor due to keyways, assumed as 1.0 due to the absence of a keyway; Kg is miscellaneous modifying factors, assumed as 1.0 for normal service conditions.

This formulation allows the estimation of the effective fatigue limit of the shaft by accounting for surface condition, size effects, reliability level, temperature, loading conditions, stress concentration, and service environment.

The unmodified fatigue limit (Se') of the shaft material was estimated based on the conventional approximation for steels, considering Se' ≈ 0.5·Su [14]. Using the ultimate tensile strength obtained from Table 2 (Su ≈ 899 MPa), the estimated fatigue limit is approximately Se' ≈ 450 MPa. This value represents the baseline fatigue resistance of the material and is subsequently modified by correction factors to account for surface finish, size, reliability, and loading conditions.

Therefore, considering that the unmodified fatigue limit of the shaft material (Se') of 450 MPa and that the shaft diameter is 380 mm, the corrected fatigue limit was calculated as Sf = 193.2 MPa. For general considerations regarding the effect of mean stress on fatigue behavior, the Goodman line is commonly adopted. Graphically, the Goodman criterion is represented by a straight line on a mean stress versus alternating stress diagram, defining the boundary between safe and failure regions. Any combination of mean and alternating stresses located below (or to the left of) the Goodman line is expected to be safe against fatigue failure, while stress states above (or to the right of) the line indicate potential fatigue failure.

The Goodman relation is given by Equation 10 and is defined by the following parameters:

$$\frac{S_a}{S_{cr}} + \frac{S_m}{\mathrm{UTS}} = 1 \quad (10)$$

Where: Sa is alternating stress, defined as $S_a = \frac{S_{max}-S_{min}}{2}$; Sm is mean stress, defined a $S_m = \frac{S_{max}+S_{min}}{2}$; Smax is maximum stress, equal to 470 MPa; Smin is minimum stress, assumed as 0 MPa; UTS is ultimate tensile strength of the material, equal to 899.6 MPa; Scr is fatigue stress corrected according to the Goodman criterion.

The maximum stress (Smax) was obtained from fracture mechanics–based calculations, considering the stress concentration effect resulting from contact with the expansion ring. The minimum stress (Smin) was assumed to represent the most severe condition, corresponding to a complete loss of contact pressure between the expansion ring and the shaft.

By substituting these values into the Goodman equation, a corrected equivalent fatigue stress of Scr = 318 MPa was obtained. This value is higher than the corrected fatigue limit of the material (Sf = 193.2 MPa). Therefore, it falls outside the safe region of the Goodman diagram, indicating a finite fatigue life condition and susceptibility to fatigue failure.

It should be noted that the fracture mechanics and fatigue analyses presented in this study rely on simplifying assumptions, including the adoption of a stress concentration factor (Kt ≈ 2) based on literature for interference-fitted assemblies, the assumption of minimum stress (Smin = 0 MPa) to represent a conservative condition, and the use of a semi-elliptical surface crack geometry. Furthermore, the threshold stress intensity factor (ΔKth) was obtained from literature data for similar steels. While these assumptions are widely accepted for engineering estimations, they introduce uncertainties that may affect the quantitative accuracy of the results. Nevertheless, they do not compromise the qualitative conclusions regarding the failure mechanism.

The safety factor represents the degree to which the maximum material strength is intentionally underestimated in order to ensure a safe design. In fatigue analyses considering mean stress effects, a single safety factor is applied simultaneously to both the alternating stress and the mean stress.

Since fatigue life estimation requires both the alternating and mean stress components, it is not possible to determine these stresses using only a single safety factor independently. Therefore, according to this criterion, the safety factor (n) is obtained from the ratio defined by Equation 11:

$$\frac{S_a}{S_f} + \frac{S_m}{S_u} = \frac{1}{n} \qquad (11)$$

where: S_f is the corrected fatigue limit of the material, equal to 193.2 MPa; n is the fatigue safety factor.

By substituting the calculated stress values into Equation 11, a safety factor of n = 0.68 was obtained, indicating that the material is subjected to a stress cycle that is likely to result in fatigue failure. When the stress amplitude exceeds the fatigue limit of the material, the fatigue life under finite-life conditions can be estimated using Basquin's equation:

$$\sigma_{eq} = Sf' \, (N_f)^b$$

Where σ_{eq} is the equivalent fully-reversed stress obtained from the Goodman relation (318 MPa), *Sf'* is the fatigue strength coefficient (1211 MPa), N_f is the number of cycles to failure and *b* is the fatigue strength exponent (-0.075). The parameters of Basquin's equation were obtained from the literature [15,16]. For low-alloy steels such as SAE 4340, the fatigue strength exponent (b) typically ranges between −0.05 and −0.12, while the fatigue strength coefficient (Sf') is generally proportional to the ultimate tensile strength, commonly 1.3 times Su. By substituting these values into the equation, a fatigue life of $N_f \approx 2.77 \times 10^7$ cycles is obtained. Considering a pulley rotational speed of 47 rpm, this corresponds to an estimated service life of approximately 408 days. Therefore, preventive replacement of the component is recommended within the estimated fatigue life interval to ensure safe operating conditions and reduce the risk of structural failure.

It is important to note that the fatigue life estimation obtained from Basquin's equation is based on an idealized condition that does not explicitly account for surface damage mechanisms. In the present case, the presence of fretting at the shaft–expansion ring interface plays a critical role in significantly reducing the fatigue life. Fretting damage promotes the formation of localized surface defects, including microcracks, plastic deformation, and increased surface roughness, which act as stress concentrators and preferential sites for crack initiation. As previously demonstrated, defects on the order of 0.113 mm are sufficient to propagate under the applied cyclic stresses. Therefore, the fatigue life predicted using nominal stress-based approaches represents an upper-bound estimation, whereas the actual service life is expected to be considerably shorter due to the presence of fretting-induced damage.

The presence of fretting damage significantly alters the local stress state and promotes early crack initiation, explaining the discrepancy between design predictions and observed failures. When such defects exist, the applied stresses can promote crack propagation, ultimately leading to fracture. Therefore, a fracture mechanics–based assessment is essential to evaluate the material behavior under these conditions.

By assuming the presence of a small defect or a surface crack of size a, with a semi-elliptical shape located at the surface of the shaft, the stress range required to drive fatigue crack propagation from a pre-existing defect can be expressed by Equation 12, as proposed by Bannantine et al [17]:

$$\Delta K_{th} = \Delta\sigma\sqrt{\pi a} \tag{12}$$

where: ΔK_{th} is the threshold stress intensity factor range for fatigue crack growth, below which crack propagation does not occur by fatigue. A value of $\Delta K_{th} = 3.9\,\mathrm{MPa}\sqrt{\mathrm{m}}$ was adopted, based on data from the literature [17].

$\Delta\sigma$ is the applied stress range required to propagate the crack (MPa), assumed as 318 MPa, corresponding to the corrected equivalent stress calculated previously a is the initial crack size (mm).

Considering that the effective stress at the failure location is expected to be higher than the value estimated under ideal ring–shaft contact conditions (Δσ = 318 MPa), the application of the above equation allows the estimation of the minimum defect size capable of promoting fatigue crack propagation. By substituting the adopted values into Equation 12, it is estimated that surface defects with sizes on the order of a ≈ 0.113 mm are sufficient to initiate and sustain fatigue crack growth.

This result indicates a high sensitivity of the shaft to small surface imperfections under the evaluated loading conditions, reinforcing the relevance of fracture mechanics–based analyses for assessing damage tolerance and failure susceptibility in interference-fitted shaft assemblies. Therefore, the contact pressures acting on the shaft generated exclusively by the expansion ring would not, by themselves, be sufficient to cause fatigue failure, since the resulting stress levels remain below the material fatigue limit. For fatigue crack propagation to occur, the presence of a microcrack with a size on the order of 0.113 mm would be required. Such a microcrack may have originated from a fretting damage mechanism, which requires the occurrence of relative motion between the expansion ring and the shaft. This mechanism was evidenced by the analyses of the contact surface between the shaft and the expansion ring, where microcracks of the same order of magnitude, as well as regions of excessive plastic deformation, were observed.

In view of the identified failure origin, attributed to the occurrence of fretting at the contact region between the shaft and the expansion ring, it is essential—until an effective corrective action is implemented (such as changing the expansion ring design, increasing the wear resistance of the shaft material, or adopting alternative mitigation measures)—to understand the defect propagation rate. Such knowledge allows the establishment of an adequate inspection and maintenance plan aimed at preventing catastrophic failure.

The crack growth rate can be evaluated using the Paris law (Equation 13), which enables the prediction of the number of loading cycles (i.e., time in service) required for a crack to grow from an initial size a_0 to a final size a_f. Equation (13) corresponds to the integrated form of the Paris law, considering a variable geometric correction factor Y as a function of crack size.

$$N = \frac{a_0^{1-\frac{m}{2}} - a_f^{1-\frac{m}{2}}}{C\left(\frac{m}{2}-1\right) Y^m (\Delta\sigma)^m \pi^{\frac{m}{2}}} \tag{13}$$

where N is the number of cycles required for crack propagation, a_0 is the initial crack size required to initiate propagation (0.113 mm, obtained from Equation 12), a_f is the final crack size measured on the shaft fracture surface (190 mm), C and m are material constants ($C = 1.3 \times 10^{-11}$, $m = 2.8$), $\Delta\sigma$ is the applied stress range driving crack propagation (318 MPa), and Y is the geometric correction factor obtained from Equation 3, which varies with crack size.

The material constants C and m used in the Paris law were obtained from literature data for quenched and tempered steels with mechanical properties comparable to SAE 4340 [18-21]. These parameters describe the fatigue crack growth behavior in the stable propagation regime (Region II of the crack growth curve). The constant C represents a material-dependent scaling factor that governs the magnitude of the crack growth rate, while the exponent m defines the sensitivity of crack propagation to the applied stress intensity factor range (ΔK). Higher values of m indicate greater sensitivity to variations in ΔK, resulting in faster crack growth under increasing loading conditions. The adopted values (C = 1.3×10^{-11} and m = 2.8) are consistent with typical ranges reported in the literature for high-strength steels under similar loading conditions, thus providing a reasonable approximation for the present analysis.

By applying the Paris law and discretizing the crack growth up to the final crack size of 190 mm, it was observed that the crack would require a number of loading cycles equivalent to approximately seven days of operation to reach the critical size. The estimated crack propagation time of approximately seven days should be interpreted as an order-of-magnitude estimation rather than an exact prediction, as it depends on material constants, loading conditions, and geometric assumptions. Variations in the Paris law parameters (C and m), as well as in the applied stress range, may significantly affect the predicted crack growth rate. Nevertheless, the result highlights the rapid propagation stage once a crack is nucleated. Based on this result, the inspection strategy should be established with intervals shorter than seven days, in order to allow the early detection of fatigue cracks and the replacement of the shaft before the crack evolves into a catastrophic failure. The estimated critical defect size (~0.113 mm) indicates high sensitivity to small surface defects, emphasizing the importance of controlling surface damage and wear processes. Combined with the rapid crack propagation stage, this finding reinforces the need for strict inspection intervals and highlights the limited tolerance of the system to fretting-induced damage. It should be noted that more advanced approaches, such as finite element analysis or detailed contact mechanics modeling, could provide a more accurate description of the stress distribution at the shaft–hub interface. However, within the scope of the present study, the analytical formulation adopted is sufficient to support the identification of the dominant failure mechanism.

4. CONCLUSIONS

The dynamic analysis of the shaft was carried out through fatigue evaluation using the Goodman correction criterion, with the results compared to the fatigue limit estimated according to the methodology proposed by CEMA (2014). The results indicated that the stress amplitudes acting on the shaft exceed the material fatigue limit, resulting in a safety factor of 0.68, which characterizes a finite fatigue life condition and susceptibility to fatigue failure.

Additionally, fatigue life was estimated based on Basquin's equation, from which an approximate service life of 408 days was obtained for the shaft under the analyzed loading conditions. However, it is important to note that this estimation is based on nominal stress conditions and does not explicitly account for surface damage mechanisms.

In practice, surface and SEM analyses revealed clear evidence of fretting damage at the shaft–expansion ring interface, characterized by microcracks, plastic deformation, and wear features. Fretting promotes the formation of localized microdefects, such as microcracks, plastic deformation, and increased surface roughness, which act as stress concentrators and significantly accelerate crack initiation. As demonstrated by the fracture mechanics analysis, defects on the order of 0.113 mm are sufficient to propagate under the applied cyclic stresses, leading to premature failure.

Therefore, the fatigue life predicted using stress-based approaches represents an upper-bound estimation, while the actual service life is governed by fretting-induced damage and crack propagation. Based on these findings, preventive replacement of the component is strongly recommended within the estimated fatigue life interval, ensuring safe operating conditions and mitigating the risk of catastrophic structural failure. Crack growth predictions based on the Paris law indicated that once initiated, a fatigue crack could reach a critical size in approximately seven days of operation. These findings confirm that the failure was caused by fretting fatigue driven by localized contact stresses and relative micro-sliding at the interference-fitted interface.

The results highlight the critical need to mitigate fretting at shaft–hub connections and provide a quantitative basis for defining corrective actions, inspection intervals, and maintenance strategies to prevent catastrophic failures in belt conveyor pulley systems. From a practical perspective, mitigation of fretting fatigue in shaft–hub connections may involve improving interference fit design to ensure more uniform contact pressure, optimizing surface finish to reduce stress concentration, and applying surface treatments or coatings to increase wear resistance. Additionally, periodic inspection intervals shorter than the estimated crack propagation period are recommended to prevent catastrophic failures.

Acknowledgement

The authors acknowledge Vale and the Vale Institute of Technology for their support and encouragement, as well as the Materials Institute of Brazil (MIB) for the characterization analyses performed.

REFERENCES

[1] N. Lovren and D. Debelić, “About the history of belt conveyors,” *Engineering Review*, vol. 28, no. 2, pp. 111–118, Dec. 2008.

[2] A. Kesimal, “Different types of belt conveyors and their applications in surface mines,” *Mineral Resources Engineering*, vol. 06, no. 04, pp. 195–219, Dec. 1997, doi: 10.1142/s0950609897000188.

[3] Conveyor Equipment Manufacturers Association, *Belt Conveyors for Bulk Materials*, 7th ed. Naples, FL, USA: Conveyor Equipment Manufacturers Association, 2014.

[4] V. Sethi and L. K. Nordell, “Modern pulley design techniques and failure analysis methods,” in *Proc. AIME-SME Annu. Meeting*, Reno, NV, USA, Feb. 15–18, 1993.

[5] T. R. Patel, R. R. Patel, and S. P. Joshi, “Conveyor pulley failure analysis,” *Int. J. Eng. Dev. Res.*, vol. 2, no. 1, pp. 445–447, Mar. 2014.

[6] A. Jain, M. K. Vishwakarma, R. S. Mulapuri, T. Thirumurugan, N. R. Kumar, and S. Ojha, “Failure analysis of Snub Pulley shell of belt conveyor,” *Journal of Failure Analysis and Prevention*, vol. 26, no. 1, pp. 4–8, Jan. 2026, doi: 10.1007/s11668-026-02377-x.

[7] A. Cecala et al., “Dust control handbook for industrial minerals mining and processing. Second edition.,” Mar. 2019. doi: 10.26616/nioshpub2019124.

[8] G. Van Zyl and A. Al-Sahli, “Failure analysis of conveyor pulley shaft,” *Case Studies in Engineering Failure Analysis*, vol. 1, no. 2, pp. 144–155, Apr. 2013, doi: 10.1016/j.csefa.2013.04.011.

[9] ASTM International, “Standard test methods for tension testing of metallic materials,” ASTM E8/E8M-21, West Conshohocken, PA, USA, 2021, doi: 10.1520/E0008_E0008M-21.

[10] ASTM International, “Standard test methods for notched bar impact testing of metallic materials,” ASTM E23-16, West Conshohocken, PA, USA, 2016, doi: 10.1520/E0023-16.

[11] J. Barsom and S. Rolfe, *Fracture and Fatigue Control in Structures: Applications of Fracture Mechanics, third edition*. 1999, doi: 10.1520/mnl41-3rd-eb.

[12] D. A. Skinn et al., *Damage Tolerant Design Handbook*. Dayton, OH, USA: University of Dayton, 1994.

[13] W. D. Pilkey, *Peterson’s Stress Concentration Factors*, 3rd ed. New York, NY, USA: John Wiley & Sons, 1997, doi: 10.1002/9780470172674.

[14] R. Motte and W. De Waele, “An overview of estimations for the High-Cycle Fatigue strength of conventionally manufactured steels based on other mechanical properties,” *Metals*, vol. 14, no. 1, p. 85, Jan. 2024, doi: 10.3390/met14010085.

[15] N. E. Dowling, K. Siva Prasad, and R. Narayanasamy, *Mechanical behavior of materials: engineering methods for deformation, fracture, and fatigue*, 4. ed., International ed. Boston, Mass.: Pearson, 2013.

[16] R. I. Stephens and H. O. Fuchs, Eds., *Metal fatigue in engineering*, 2. ed. in A Wiley-Interscience publication. New York Weinheim: Wiley, 2001.

[17] J. A. Bannantine, J. J. Comer, and J. L. Handrock, *Fundamentals of metal fatigue analysis*. Upper Saddle River, NJ: Prentice Hall, 1990.

[18] S. K. Putatunda, S. Bajaj, and J. Boileau, A Novel Method for Determining the Fatigue Threshold and Fracture Toughness from a Single Test," *International Journal of Metallurgy and Metal Physics*, vol. 3, no. 2, Dec. 2018, doi: 10.35840/2631-5076/9223.

[19] F. A. Heiser and W. Mortimer, "Effect of thickness and orientation on fatigue crack growth rate in 4340 steel," *Metallurgical Transactions*, vol. 3, no. 8, pp. 2119–2123, Aug. 1972, doi: 10.1007/bf02643221.

[20] E. J. Imhof and J. M. Barsom, "Fatigue and Corrosion-Fatigue Crack Growth of 4340 Steel at Various Yield Strengths," in *Progress in Flaw Growth and Fracture Toughness Testing*, ASTM STP 536, 1973, pp. 182–205, doi: 10.1520/STP49720S.

[21] S. K. Putatunda and J. M. Rigsbee, "Effect of specimen size on fatigue crack growth rate in AISI 4340 steel," *Engineering Fracture Mechanics*, vol. 22, no. 2, pp. 335–345, Jan. 1985, doi: 10.1016/s0013-7944(85)80034-5.